

# Structure calculation strategies for membrane proteins; a comparison study

Ileana Stoica\*  
National Research Council of Canada  
6100 Royalmount Ave.  
Montréal, QC, H4P 2R2, Canada

November 19, 2018

## Abstract

Structure predictions of helical membrane proteins have been designed to take advantage of the structural autonomy of secondary structure elements, as postulated by the two-stage model of Engelman and Popot. In this context, we investigate structure calculation strategies for two membrane proteins with different functions, sizes, aminoacid compositions, and topologies: the glycoporphin A homodimer (a paradigm for close inter-helical packing in membrane proteins) and aquaporin (a channel protein). Our structure calculations are based on two alternative folding schemes: a one-step simulated annealing from an extended chain conformation, and a two-step procedure inspired by the grid-search methods traditionally used in membrane protein predictions. In this framework, we investigate rationales for the utilization of sparse NMR data such as distance-based restraints and residual dipolar couplings in structure calculations of helical membrane proteins.

**Keywords:** membrane protein; transmembrane helix; NMR structure calculation; glycoporphin A; aquaporin

## 1 Introduction

A vastly used frame for understanding membrane protein synthesis and folding is the two-stage model.

First introduced by Popot and Engelman ([1]) and further elaborated by White and Wimley ([2]), the model proposes that the stable conformation of a multi-spanning helical membrane protein is reached by interactions between pre-folded transmembrane (TM) helices, without changes in the helical secondary structure. Typically, membrane protein structure predictions are "two-step" conformational searches and follow conceptually the two-stage model ([3, 4, 5]). The assignment

---

\*E-mail address: ileana@bri.nrc.ca

of individual transmembrane helices is the first step towards the prediction of a membrane protein conformation ([3, 4, 5]). It is usually considered that the success of membrane protein prediction is largely determined by meeting the second challenge, of correctly packing individually pre-folded helices ([3, 4, 5]).

In membrane protein predictions, grid searches of the helical bundle conformational space focus on helix-helix interactions and assume a rigid canonical  $\alpha$ -helical backbone, in view of the two-stage model of membrane protein folding ([5, 6, 7, 8]).

Early conformational searches of the dimeric transmembrane region of Glycophorin A from human erythrocytes have been designed to take advantage of the secondary structure autonomy of individual helices ([6, 7]). These and subsequent studies of other membrane proteins such as the phospholamban homo-pentamer consisted of multiple short *in vacuo* molecular dynamics simulations with different starting positions to ensure a comprehensive sampling of the helix-helix interaction space. Energy was used as a discriminating tool for selecting clusters of most probable conformations ([4]), while data coming from mutational analysis, NOESY experiments, cross-linking studies, and CD-FTIR were used as an additional selection criterion, and to reduce the complexity of the search ([4, 6, 7, 8, 9, 10, 11]).

The pioneering work on the glycoporphin A ([6, 7]), as well as more recent simulations on helical membrane proteins such as the integrin homo-oligomer ([12]), the Influenza virus A M2 proton channel and the HIV vpu ([4]), and EmrE - the multi-drug transporter from E.coli ([13]), are beautiful demonstrations of the predictive power of the computational approach in membrane protein structure determination.

At the same time, an exhaustive search of the helical bundle conformational space may become computationally expensive, especially if symmetry considerations cannot be applied (the case of hetero-oligomeric proteins). One way to overcome some of the difficulties related to conformational sampling is to incorporate topological restraints in the structure prediction/calculation procedure ([14]).

Alternatively, constraints such as those obtained from chemical cross-linking, fluorescence resonance energy transfer (FRET), disulfide mapping, NMR, and site-directed spin labeling combined with EPR can be incorporated in the design of penalty functions that retrieve near-native conformations of helical bundles from a collection of misfolded structures ([15]). In these approaches, the experimental distance restraints are used in conjunction with structural rules derived from the analysis of helix-helix interactions in known protein structures ([4]).

The current work focuses on structure calculation strategies with sparse NMR data. The most vastly used NMR restraints are distance-based restraints which can be obtained from Nuclear Overhauser Experiments (NOE), and backbone and sidechain dihedral angle restraints which can be extracted from coupling data. More recently, global alignment restraints in the form of residual dipolar couplings (RDC-s) have been proved to substantially refine protein structures or even provide reliable predictions in the presence of sparse NOE data ([16]).

It has been shown ([17, 18, 19]) that protonated methyl groups offer substantial structural information and thus significantly contribute to NMR protein structure determination. With the advances in multidimensional NMR spectroscopy, it has become possible to assign backbone and side chain resonances in highly deuterated, selectively methyl-protonated proteins, some of them of high molecular weight ([17, 18]). Resonances from selectively methyl-protonated hydrophobic residues can be especially useful in membrane protein calculations, given that the most impor-

tant characteristic of transmembrane helices (which makes them readily detectable as secondary structure elements) is their hydrophobicity ([20]). Moreover, oligomerization and helix packing in membrane proteins usually involve hydrophobic motifs; glycophorin A is a paradigm for helical packing and dimerization mediated by such a motif ([1, 3, 20, 21, 22]).

In the present study we explore structure calculation strategies for helical membrane proteins. Our purpose is to develop a rational approach for the utilization of a minimal data set of restraints that can be obtained by solution NMR. We aim to tailor our computations to helical membrane proteins; therefore, we start by acknowledging the importance of single transmembrane helix structure calculations. We address the issue of helical canonicity and investigate the role of NMR data in accurately predicting folds of single membrane-spanning helices. We then identify ways in which the analysis of NMR data such as NOE-s and residual dipolar couplings (RDC-s) can offer insight into helix packing in membrane proteins. The third step is to assemble the single-helix calculations and the information on inter-helical interactions into a whole-protein structure calculation. While doing that, we seek to take advantage of some features of the grid-search approach that have proved so powerful in membrane protein predictions. We use a two-step approach whereby helix-helix packing is pursued in an independent rigid-body simulated annealing refinement against inter-helical NOE-s, and then compare the results to a set of standard all-protein extended chain simulations.

## 2 Methods

### 2.1 The proteins studied

We start with structure calculations on glycophorin A. Glycophorin A (GpA) is the only homooligomerizing helical structure that has been solved so far. The GpA homodimer has often been used as a model system for the study of transmembrane helix structure and association ([21, 22]). The GpA dimer was first predicted computationally by Treutlein et al ([6]), using results from mutagenesis studies ([10, 11]) to narrow the search. The prediction was later refined, using an improved global search method ([7]). The most recent structure of the dimeric transmembrane domain of glycophorin A (GpA), in dodecyl phosphocholine micelles, was determined by NMR spectroscopy by MacKenzie et al ([23]), and provided excellent agreement with the computational predictions. Glycophorin A is a largely studied example of close inter-helical packing in membrane proteins ([20]). Two largely preformed helical surfaces associate to form the stable dimer, with a minimal loss of conformational entropy, as postulated by the two-stage model ([20]).

Channel proteins possess special features that have to be accommodated by the two-stage model ([1]): their partially polar backbones interact to sequester away a transmembrane space from the lipid environment. This requires that the unfavorable energy of creating a water-filled channel from fully folded transmembrane helices is compensated for by the energy of oligomeric association ([1]). The aquaporin family of proteins is involved in the permeation of hydrophilic molecules across membranes. Modeling the human water channel protein with the sequence-related glycerol facilitator coordinates (GlpF- [24]) provided a first atomic model for aquaporin ([25]). The atomic structure of bovine aquaporin was independently determined by X-ray analysis ([26]). Along with structural insights, molecular dynamics simulations by two different groups ([27, 28]) have elucidated essential aspects of water transport and selectivity in aquaporin. The water channel

protein is a tetramer, each monomer containing six tilted, bilayer-spanning helices and two non-spanning short helices - a functionally critical motif ([29]).

## 2.2 Computing the NMR restraints

### 2.2.1 Dihedral angles, hydrogen bonds, and inter-helical distance restraints:

To generate canonical helices from extended conformations, we enforced backbone ( $\Phi, \Psi$ ) dihedral angle assignments by placing small bounds around the canonical values ( $-57^\circ \pm 5^\circ$ ,  $-47^\circ \pm 10^\circ$ ).  $N_i - O_{i+4}$  hydrogen bonds were also added to the restraint set, with a 2.99Å target value and a 0.5Å margin, to avoid over-constraining (see [30] for a statistics of hydrogen bond parameters).

The initial NOE list comprised distances below 5.0Å (amide-amide, amide-methyl) or 6.5Å (methyl-methyl) between all amide or methyl positions that would be protonated in a deuterated, Ala, Val, Leu and Ile ( $\delta 1$  only) - methyl protonated sample ([19]).

The restraints were then assigned to one of three distance bins, corresponding to strong, medium and weak NOE resonances, respectively. Strong resonances (distances between 1.8Å and 3.5Å) were assigned a 3.0Å target value with 1.2Å and 1.0Å lower and upper bounds, respectively. Medium resonances (between 3.5Å and 4.5Å) were assigned a value of 4.0Å, with margins of 1.2Å. Weak resonances (between 4.5Å and 6.0Å) were assigned a 5.2Å value, with more relaxed margins of 1.5Å (lower bound) and 2.0Å (upper bound). All the assignments were performed non-redundantly (no pair of protons appeared twice in the restraint list). Methyl groups were treated as pseudoatoms. Only HN(i) - HN(i+1) and HN(i) - HN(i+2) distances were used for the amide proton list. No intra-residue resonances were considered. In the case of the Glycophorin A dimer, inter-monomer resonances were ascribed non-ambiguously (labeled according to the residue number and chain ID).

Subsequently, distance and residue- based criteria were used to prune the tabulated restraint list to an experimentally realistic data set. The distance-based selection criterion presented by Gardner and Kay, and extracted from actual frequencies of observation for various resonances in experimental spectra, was used as a reference ([17, 18]). Thus, sparser NOE sets were obtained by retaining only 2/3 of the “weak” resonances, or 2/3 of the “medium” resonances and 1/4 of the “weak” ones. The GpA inter-chain NOE-s involved the following residues: Leu 75, Ile 76, Val 80, Val 84, Thr 87, and Ile 88. The number of inter-helical NOE-s was varied from 21 to 4 with the help of the selection criterion described above. The BMRB-deposited NOE data set collected on GpA samples by MacKenzie et al ([23]) includes 12 non-ambiguous inter-helical distances comprising a similar stretch of residues, which have been identified by mutation analysis to be critical in helix-helix packing and dimerization ([10, 11]).

In aquaporin, sets of 348 and 115 distance restraints were designed using the selective methyl labeling pattern, between a total of 8 helices, 10 residues or more each: the 6 membrane-spanning helices, and the two connecting helices that enter half-way through the membrane. In structure calculations that focused on the TM helical bundle, the 115 NOE data set was further pruned to 92 resonances, corresponding to inter-helical distances between the 6 TM segments only.

### 2.2.2 Computation of RDC-s:

The residual dipolar coupling  $D_{AB}$  between spin 1/2 nuclei A and B (e.g. H and N) is given by ([31, 32]):

$$D_{AB} \approx -\gamma_A\gamma_B S \langle 1/r_{AB}^3 \rangle > D_a [(3\cos^2\theta_{AB} - 1) + 3/2R\sin^2\theta_{AB}\cos(2\Phi_{AB})] \quad (1)$$

where  $\gamma_A$  and  $\gamma_B$  are the gyromagnetic ratios of the two nuclei,  $r_{AB}$  is the distance between the nuclei,  $S$  is the generalized order parameter of the dipolar vector and reflects averaging due to fast local dynamics, and  $(\theta_{AB}, \Phi_{AB})$  are the polar angles describing the orientation of the internuclear bond vector AB in the alignment coordinate frame.  $D_a$  and  $R$  are the axial and rhombic components of the alignment tensor, respectively. In practice, the parameters needed by the CNS ([33]) and X-Plor ([34]) SANI (susceptibility anisotropy) module are only  $D_a$  and  $R$ .

A Fortran program was written to compute residual dipolar couplings using as alignment frame the principal axes of the molecular moment of inertia tensor  $I$ ; the program also computes the rhombicity  $R$  using the moment of inertia eigenvalues, for a given value of  $D_a$  (a  $D_a$  of 10Hz was used throughout all of the tests). For consistency, the sign of the calculated  $D_{a(HN)}$  is in agreement with the negative sign of the  $J_{HN}$  couplings. The rhombicity  $R$  was calculated as:

$$R = \frac{D_r}{D_a} = \frac{I_{xx} - I_{yy}}{I_{zz} - \frac{I_{xx} + I_{yy}}{2I_{zz}}} \quad (2)$$

where  $I_{\alpha\beta}(\alpha, \beta = x, y, z)$  are the eigenvalues of the moment of inertia tensor (ordered such as  $I_{zz} > I_{xx} > I_{yy}$ ). The set of H-N RDC-s generated with the in-house routine was then used as initial guess for a Pales ([35]) fit to the 3D structure; to match the range of  $D_{NH}$  values computed with  $D_a=10\text{Hz}$ , a bicelle concentration of 2.5% w/v was used for Pales. For consistency purposes, the dipolar coupling tensor axis was then re-cast (also with Pales) into the new (Pales-computed) alignment frame. Subsequently, during the TAD simulations, the orientation of the alignment axes was allowed to float.

## 2.3 The simulation protocols

### 2.3.1 Rigid-body/torsion angle annealing:

For the two-step procedure, the TM helices were first folded independently from fully randomized chains. For this, the CNS (Brünger et al, [33]) torsion angle dynamics anneal.inp file was used, with the standard settings, and with a Cartesian cooling stage added to the TAD slow-cool. The force constants on the NOE and dihedral angle restraints were kept constant, at 150kcal/mol  $A^2$  and 200 kcal/mol  $deg^2$  respectively, while those on the residual dipolar couplings were ramped up from 0.03 to 0.6 kcal/mol  $Hz^2$  ([36]). Canonical dihedral angles and hydrogen bond restraints were assigned as described previously.

The Xplor-NIH package ([34]) was used for the conjoined rigid-body torsion angle simulations with canonical helices. The first of the two annealing schedules described by Clore and Bewley ([37]) was used with minimal modifications. The rigid groups were comprised of the backbone atoms of the helical residues, while side chains were given full torsional freedom. The only restraints used at this stage were the inter-helical NOE-s.

The rigid body/torsion angle protocol started with a high-temperature (3500K) internal dynamics run to promote convergence, followed by 10 cycles of dynamics with van der Waals repulsion turned on, and then by slow-cool from 3500K to 100K, in 25K-temperature steps (136 cycles), each of 1,000 steps, with a fixed time step of 10fs. The force constants for the nonbonded interactions

were: 4kcal/mol for the van der Waals term, with a radius scale factor ramped geometrically from 0.4 to 0.8, and 4 kcal/mol  $deg^2$  for the torsion angle energy. For the inter-monomer NOE restraints, force constants were set to 20 kcal/mol  $A^2$  during the high-temperature stage and ramped from 100 to 450 kcal/mol  $A^2$  during the cooling stage. Following slow-cooling, 1000 steps of rigid-body minimization were performed, with the final values of force constants from the cooling phase.

For the simulations reported in Fig.7 and 8, a higher temperature of 5000K was used to improve sampling, and 5000 cooling steps were employed. Results are reported on 100 structure ensembles. Variations of the two-step rigid-body scheme included the incorporation of attractive van der Waals and electrostatic interactions to mimic the low-dielectric membrane environment. After the high-temperature search and the slow-cooling stage with a purely repulsive van der Waals term, 5000 steps of constant-temperature (300K) molecular dynamics stage and a final minimization were carried out, all including Lennard-Jones interactions and electrostatics. The parameters used for the Cartesian molecular dynamics were similar to those used by Adams et al ([7, 8]): a non-bonded cut-off of 12.5A; a switching function was applied to the van der Waals terms between 10.5 and 11.5A, and a dielectric constant of 2 was used for the cell membrane. The time step was 2fs.

### 2.3.2 Standard torsion angle dynamics (TAD) annealing:

We compare the predictions of the two-step approach to standard structure calculations from an extended conformation, which we will refer to as "the one-step procedure". To carry out "one-step" all-protein structure calculations we used the torsion angle dynamics ([38]) standard annealing protocol of CNS ([33]). Most of the force constants were set to the default parameters in the CNS anneal.inp module. The same canonical dihedral angle assignments, hydrogen bonds, RDC-s and inter-helical NOE-s were used as in the two-step rigid-body simulations. During the cooling stages, the force constants on the NOE-s, dihedral angles and SANI were chosen to match those used in the two-step procedure. For single-chain simulations, 2000 TAD cooling steps and 3000 Cartesian steps were used, while for whole-protein calculations, the number of slow-cool TAD steps was increased to 10,000 to improve convergence. All simulations started from fully extended chains; 100 structure ensembles were generated, out of which the 10 lowest energy structures were used to compute the average backbone accuracy. The ensemble accuracy is defined as the mean helical backbone RMSD relative to the reference (PDB) coordinates, as calculated by MOLMOL ([39]).

## 3 Results and discussion

### 3.1 Single TM segment calculations; the role of RDC-s

In a set of preliminary single-chain simulations, we concluded that the most efficient approach to single TM helix calculations is the strong imposition of canonical dihedral angle restraints and hydrogen bonds, in conjunction with RDC-s. This strategy eliminates the need for intra-helical distances, thus considerably reducing the number of necessary NOE assignments. The procedure yields a backbone RMSD around 1A per TM helix (20 - 30 residues), which becomes an implicit source of RMS deviations in two-step conformational searches starting with independently folded TM segments. We noticed that using RDC-s to enforce alignment of N-H bonds about the helical axis generally helped "correct" the backbone dihedral angles towards their "true" (native-structure)

<b>Protein and helix</b>	<b>Number of residues in the helix</b>	<b>Ensemble accuracy (Å) with RDC-s</b>	<b>Ensemble accuracy (Å) without RDC-s</b>
GpA monomer	27	0.91 +/- 0.14	1.26 +/- 0.16
AQP1 TM helix 1	30	1.23 +/- 0.49	1.65 +/- 0.33
AQP1 TM helix 2	25	2.36 +/- 0.32	2.33 +/- 0.26
AQP1 TM helix 3	27	1.21 +/- 0.36	0.98 +/- 0.1
AQP1 TM helix 4	19	0.44 +/- 0.04	0.85 +/- 0.29
AQP1 TM helix 5	22	1.77 +/- 0.05	2.17 +/- 0.13
AQP1 TM helix 6	20	0.72 +/- 0.03	1.22 +/- 0.11

Table 1: Structure calculations of single transmembrane helices from extended chains with canonical restraints (dihedral angles, hydrogen bonds) and with or without dipolar couplings. The following coordinates were used as reference for RMSD calculations: human glycoporphin A (PDB code: 1AFO, structure 1 of the NMR ensemble of MacKenzie et al ([23], 1997), and bovine aquaporin (1J4N, X-ray structure, 2.2Å resolution, Sui et al [26]). RMSD-s are calculated on the 10 lowest energy structures out of 100 structure ensembles.

values, thus alleviating the deviations arising from imposition of canonicity (Table 1). This was certainly the case of the GpA dimer, which has in fact been calculated in the original NMR structural determination ([23]) with canonical DA-s.

In transporters and channels the presence of non-canonical helices is linked to the existence of polar aminoacids with functional roles ([40]). Thus, it is to be expected that for some membrane proteins the imposition of canonical backbone dihedrals will result in helical topologies with poor accuracies. Moreover, we typically detect a breakdown for refinement by RDC-s, corresponding to a backbone RMSD threshold of 1-2Å per TM helix (result not shown). Consequently, helical conformations with poor accuracies are unlikely to be improved by the inclusion of dipolar couplings, if no additional restraints such as intra-chain NOE-s are used. As an example we show the aquaporin TM helix 2 (Table 1), whose C-terminus significantly deviates from the expected backbone dihedral angles. For instance, Val 69 and Ser 73 have  $\Phi$ -angles more than 60 degrees lower than the rest of the helix. The segment is however identified as a "certain" (score: 1.296) transmembrane  $\alpha$ -helix from sequence information by the TopPred ([41]) predictor. As can be seen in Table 1, RDC-s fail to improve the structure of this helix.

To further highlight the role of RDC-s in single-chain structure calculations, we examine the sensitivity of our simulated dipolar couplings to backbone helical deviations from native conformation and/or from canonical topologies. It is established experimentally that the periodic variation of the magnitudes of dipolar couplings in the backbone of a protein as a function of the residue number is linked to the periodicity inherent in regular secondary structure elements ([42]). Thus, periodicities in RDC-s known as "dipolar waves" can be used to identify helices, deviations from ideal helical topologies, and to orient helices relative to an external axis ([42]). In fact, molecular fragment replacement methods have been designed ([16]) which identify the fold of protein fragments from sets of dipolar couplings by searching a database ([16]). In structure calculation

studies, the agreement between dipolar coupling data and the molecular structure is often assessed by the parameter ([16, 43]):

$$\chi = \sqrt{\sum (D^{sim} - D^{ref})^2} \quad (3)$$

where the summation runs over the simulated set of DC-s, and the reference values are typically the experimental ones (in our case, calculated from the atomic coordinates). We select two helices (one from each protein) to illustrate the RDC sensitivity to deviations in helical topologies, as compared to the reference (PDB) structure (Fig.1).

We also include as an upper limit the  $\chi$  values that would correspond to extended chains (fully randomized conformations) of identical aminoacid sequences (Fig.1). As can be seen in Fig.1, simulated RDC-s are sensitive to deviations of the helical backbone from “ideal” topologies; a  $\chi$  of 25Hz corresponds to a canonical helical topology (helical backbone RMSD around 1Å).

## 3.2 Helix packing; the role of RDC-s and distance-based restraints

### 3.2.1 Inter-helical distances (contacts):

An interesting question concerning inter-helix packing in membrane proteins is whether TM helices pack preferentially against sequence neighbors ([4, 44]).

To critically evaluate our simulated inter-helical NOE restraints, we analyzed this question for aquaporin, while also performing a statistics over several transporter/channel proteins for better comparison. With the particular labeling pattern used in our study, inter-helical NOE-s involve predominantly the hydrophobic aminoacids. We therefore do not expect our inter-helical NOE pattern to offer a perfect description of helix-helix interactions in protein channels for instance, where functionally important polar residues are often placed at the helical interfaces ([20, 40]). However, as can be seen in Fig.2, the methyl labeling pattern applied to aquaporin does reveal the existence of a significant number of NOE-s between non-consecutive pairs of TM helices.

Indeed, a small statistics of backbone inter-helical contacts over 6 transporter and channel proteins among which aquaporin (Fig.3) revealed that, in fact, aquaporin has the highest fraction of contacts between helices separated by 1 or more TM helices down the sequence, which is well captured by the NOE pattern presented in Fig.2.

We also note that the incorporation of distance restraints involving the two partially inserted helices of AQP1 has a significant impact on the accuracy of the calculated structure (see below). This may be useful in modeling pairs of helices involved in extensive contacts in multi-spanning helical proteins.

### 3.2.2 Helix crossing angles:

In the early GpA conformational searches ([6]),  $\Omega = +/- 45^\circ$  helix crossing angles were chosen as the optimal starting angles, as they allowed convergence to stable right-handed coils. However, subsequent studies showed that stable configurations could be identified by extensive sampling of the entire space defined by the helical rotational degrees. In cases more complex than the glycoporphin homodimer (e.g. bundles of many non-identical helices) it may be more important to have a good initial guess for crossing angles between pairs of helices, as exhaustive conformational searches become expensive.

In Fig.4 we use simulated RDC data for such an initial guess. To extract crossing angles from the RDC data, we used Pales ([35]) and our RDC initial guess to compute the alignment frame for each of the two helices individually, then computed the tilt of each helix with respect to the laboratory z-axis from the alignment tensor eigenvectors. We thus obtained a crossing angle for the homodimer. By starting with increasingly distorted helical backbones (with respect to the PDB structure), we estimated the degree of over- or under-prediction of the helix crossing angle for "non-ideal" helical segments. The calculation is fairly robust to non-canonicity issues; the estimated crossing angles proved to be affected by the quality of the individual helices only to a limited extent (Fig.4). There remains the redundancy associated with the parallel/anti-parallel orientation of the helices, which can be resolved from inspection of the inter-helical NOE-s, and that associated with the handedness of the coil (the sign of  $\Omega$ ), which as we show later does not bias the results of the two-step method (see the Results of the two-step procedure).

### 3.3 Assembling the intra- and inter-helical information; simulations from pre-folded helices

As postulated by the two-stage model, the second stage of membrane protein folding is the packing of pre-formed trans-bilayer helices. To this end, we performed a simulated annealing search for identifying the optimal relative orientation of pre-folded helices. Recognizing that a force field-guided grid search which relies upon the convergence of different starting structures to particular energy minima may suffer from poor convergence in the absence of experimental data ([4]), we used inter-helical NOE restraints to aid the simulated annealing search. We note in the single TM segment section that the folding of individual chains relies heavily on backbone dihedral angles, hydrogen bonds, and RDC-s. No intra-helical NOE-s are needed at this stage ("stage one" in membrane protein folding). In stage two, the only NMR data used to guide the search towards a stable conformation are inter-helical NOE-s, while the helical backbones are kept rigid. In our tests, the procedure implies a 10-fold or more reduction in the number of resonances that can be used in the structure determination, with the methyl labeling pattern.

#### 3.3.1 Incorporation of attractive van der Waals and electrostatic energies:

We examined the result of including a final stage, of molecular dynamics with Lennard-Jones and electrostatic interactions, at the end of the conjoined rigid-body/torsion angle simulated annealing. In this fashion we attempted to improve accuracy by more realistically sampling helix-helix packing interactions. Attractive van der Waals and electrostatic terms were parametrized as described in the Methods section. When a protein is modeled as rigid, the reorientation of internal groups does contribute to the dielectric constant, unlike in free molecular dynamics, for instance, where all reorientations of dipolar groups within the protein are included explicitly in the simulation ([45]). This observation makes the choice of the internal dielectric constant in rigid-body simulations a tricky issue. In the present simulations, dielectric constants of 2 and 10 were used to mimic the lipid environment. The differences in the final ensemble-averaged accuracies were less than 0.2Å. Torres et al also note that results are virtually indistinguishable for  $\epsilon=1$  and  $\epsilon=2$  ([4]). In Fig.5 are shown results obtained from initially parallel helices, with varying degrees of backbone RMS deviation from the PDB coordinates; a value of  $\epsilon=2$  ([46]) was used for these calculations.

If helices were significantly distorted (more than 2Å backbone RMSD per helix), the improvement in ensemble accuracy upon inclusion of electrostatic and attractive van der Waals forces was negligible (fell within the ensemble variance). On the other hand, the improvement was sizable for “canonical” helices (RMSD around 1Å per helix). In such cases, the positive effect of the final molecular dynamics round emphasizes the role that inter-helical energies play, along with experimental restraints, in guiding the search for stable conformations of  $\alpha$ -helical bundles. We therefore chose to include the constant-temperature molecular dynamics stage in all subsequent rigid-body conformational searches.

### 3.3.2 Results of the two-step folding simulations:

In the first set of GpA simulations, we started with canonical helices (generated as described in Methods), which were then placed at 20-24Å apart (measured between the  $\alpha$ -Carbons of Gly 83). We varied the helix crossing angle  $\Omega$ , which in the case of a homodimer is double the helix tilt angle, from  $-90^\circ$  to  $90^\circ$  and covering both the right (negative) and the left (positive) handedness.

The first main conclusion of our two-step structure calculations on GpA is that the success of the rigid-body refinement is significantly dependent on the quality of the predicted individual helices (Fig.5) and less dependent on the helix-helix relative orientation in the starting structure (Fig.6). Using the initial guess provided by the RDC data on the pair of canonical helices (crossing angles around  $\pm 45^\circ$ , see Fig.4) proved to offer a slight advantage in accuracy (Fig.6). The problem of identifying the correct handedness of the dimer also appears to be solved by the rigid-body procedure: while we do occasionally see low energy left-handed dimers, we note that the lowest energy ensemble has a majority of right-handed helices, irrespective of the initial handedness (sign of  $\Omega$ ). By non-redundantly re-numbering residues in the two GpA chains (for NOE assignment purposes - see Methods), our RMSD calculation (as well as visual inspection) includes the handedness of the helix pairs, thus providing an implicit assessment the correct handedness.

As the initial crossing angle was varied between  $-90^\circ$  and  $+90^\circ$ , a difference of less than 1Å in ensemble accuracies was spanned. The mean ensemble accuracies are about 1Å better than the TAD ensemble accuracies (around 2Å) obtained by constraining  $\alpha$ -helical dihedral angles to canonical values, and using the same 10 inter-helical NOE-s (Fig.7).

Finally, we report the performances of the two structure calculation strategies (one and two-step) for our model proteins (Fig.7 and 8).

For GpA the two-step annealing of parallel prefolded helices is the best route towards an accurate global fold. The two-step procedure is also computationally inexpensive, since only one independent single-chain SA is needed in the first step to produce the starting canonical helices. Increasing the number of inter-helical NOE-s by including more long-range restraints (up to 6.5Å) improved the accuracy, while decreasing it dramatically reduced the quality of the calculated folds (Fig.7). With enforced canonical DA-s, variations in the number of intra-helical NOE-s (achieved by placing different ratios corresponding to frequencies of observation for medium and weak resonances, as described in the Methods section) had a negligible impact, falling within the ensemble variance. Different levels of DA imposition (rigid, strong, medium) had a modest impact on the helical fold, possibly due to the presence of hydrogen bonds which hold together the helical backbone. Overall, our simulations suggest that the assumption of canonical topologies for the monomers, together with the extraction of the maximum possible number of inter-helical distance restraints, is the best

structure calculation strategy for GpA. In this context, the exploration of other labeling methods, including the use of paramagnetic spin probes for longer-range distances, may provide even better folds.

In the aquaporin conjoined rigid-body/torsion angle simulations, the individual TM helices were folded separately from extended chains as described previously, using RDC-s in addition to canonical DA-s. The starting helices were picked from the TAD ensembles whose average accuracies are listed in Table 1. Rigid-body refinement was then performed against the 92 inter-helical NOE-s, as described in the Methods section. For the corresponding one-step structure calculations from an extended chain, the same inter-helical NOE-s were used as in the two-step procedure.

In aquaporin, the two-step procedure gave poor accuracies (Fig.8). The size of the protein is definitely an issue, as typically successful applications of the grid-search methods have been reported for homo-oligomers ([9, 12, 13]), but not for bundles of 6 non-identical TM helices. Other factors are the inter-helical packing pattern (Fig.3) and the non-canoncity of some of the aquaporin TM helices (Table 1). The average ensemble accuracy can be roughly approximated by the number of TM helices times the average backbone RMSD per helix (with respect to canonical  $\alpha$ -helices of identical aminoacid sequences). For membrane proteins such as aquaporin, different labeling patterns and longer-range distance constraints (such as those that can be obtained with paramagnetic probes) will be needed to improve the quality of the fold with the two-step procedure. As suggested previously, RDC-s can also be used for a reliable initial guess of the crossing angles between pairs of TM helices.

The best folding strategy for the water channel was found to be the “one-step” procedure with canonical DA restraints, hydrogen bonds, and as many inter-helical NOE-s as available with our labeling pattern. Fundamentally, the result is in agreement with the GpA conclusions: membrane proteins of different sizes, topologies and functionalities can be accurately folded by restraining helices into canonical formations and focusing on the exhaustive assignment of inter-helical resonances (preferably longer-range). Adding intra-helical NOE-s does not bring visible improvements (Fig.8).

Neither does changing the DA assignments to other target values: A statistics over 160 transmembrane helices from 15 high-resolution X-ray structures has provided an average value of ( $-60.7^\circ \pm 11.7^\circ$ ,  $-44.7^\circ \pm 13.0^\circ$ ) for the helical ( $\Phi, \Psi$ ) angles in channel proteins and solute transporters ([47]). In the case of aquaporin we examined the impact of introducing transporter/channel specific values in the dihedral angle assignments. Tuning the target ( $\Phi, \Psi$ ) helical dihedral angles towards protein class-average values did not produce an improvement in the accuracy of the global fold (Fig.8).

In the previous paragraphs we emphasized the similarity between the two test case proteins. While indeed both GpA and AQP1 calculations recommend the same strategy conceptually (canonical helices, exhaustive inter-helical assignments), the winning computational approaches are different. Our simulations suggest that GpA calculations benefit from the two-stage model assumption of secondary structure autonomy, while aquaporin helices need to be folded concertedly, technically speaking: intra- and inter-helical forces need to be sampled together. Moreover, the role of the two non-spanning helices is also highlighted in the AQP1 calculation, as their omission results in poor accuracies (Fig.8). This finding relates very well to the observation of Sale et al ([15]) concerning the application of a scoring function comprising a variety of sparse distance restraints to a set of six known membrane protein structures, among which aquaporin. Aquaporin posed the biggest

challenge to the approach, which authors attribute to the removal of contact penalties involving the two non-spanning helices ([15]).

## 4 Conclusions

If canonical topologies are assumed for membrane-spanning helices as is the case in most grid-search procedures ([6, 7, 8, 9, 12, 13]), the number of distance-based restraints that can be extracted from a typical solution NMR spectrum can be significantly reduced to a subset containing mostly inter-helical NOE-s. The assumption is that TM  $\alpha$ -helices can be reliably identified (by dipolar waves, hydrophathy searches or chemical shift assignment) and adequately constrained with a combination of dihedral angles and hydrogen bonds. To compensate for an inaccurate TM helix prediction or more importantly for deviations from canonicity, residual dipolar couplings will be needed.

An average of 10 inter-helical NOE-s per pair of TM segments, with the selective methyl labeling pattern considered in the present study, resulted in medium resolution structures for GpA (1Å - 2.5Å accuracies). The procedure implies a significant (20-fold) reduction in the number of resonances necessary, thus eliminating the need for exhaustive intra-helical NOE assignment. Our results also recommend the use of other techniques such as spin labeling for the extraction of longer-range inter-helical distance restraints.

A canonical homodimer, GpA is best folded using the “two-step” method, inspired by the two-stage model of membrane synthesis and folding ([1]). The procedure benefits from a more realistic modeling of packing forces in a final short round of MD, as well as (slightly) from an initial guess of the helical crossing angle.

For a bundle of non-identical and non-canonical TM segments such as the “hourglass” topology of aquaporin, the overall resolution of the two-step method is low and scales almost linearly with the number of TM helices. The success of the “one-step” strategy suggests that in the water channel protein, unlike in GpA, helices need to be folded and packed concertedly. Still, for aquaporin as for glycophorin A, the imposition of canonical helical topologies, combined with the exhaustive assignment of (long-range) inter-helical NOE-s, was found to be the best structure calculation strategy with sparse NMR data.

## 5 Acknowledgments

This work was started at the Univ. of Ottawa. The author wishes to gratefully acknowledge Dr. Natalie Goto for valuable discussions and for an NMR spectroscopist’s perspective.

## References

- [1] Popot, J.-L.; Engelman, D. M. *Biochemistry* 1990, 29, 4031-4037.
- [2] White, S. H.; Wimley, W. C. *Annu Rev Biophys Biomol Struct* 1999, 28, 319-365.
- [3] DeGrado, W. F.; Gratkowski, H.; Lear, J. D. *Prot Sci* 2003, 12, 647-665.
- [4] Torres, J.; Kukol, A.; Arkin, I. T. *Biophys J* 2001, 81, 2681-2692.

- [5] Bowie, J. U. *J Mol Biol* 1997, 272, 780-789.
- [6] Treutlein, H. R.; Lemmon, M. A.; Engelman, D. M.; Brünger, A. T. *Biochemistry* 1992, 31, 12726-12732.
- [7] Adams, P. D.; Engelman, D. M.; Brünger, A. T. *Proteins: Struct Funct Genet* 1996, 26, 257-261.
- [8] Adams, P. D.; Arkin, I. T.; Engelman, D. M.; Brünger, A. T. *Nat Struct Biol* 1995, 2, 154-162.
- [9] Arkin, I.; Adams, P.; Brünger, A.; Smith, S.; Engelman, D. *Annu Rev Biophys Biomol Struct* 1997, 26, 157-159.
- [10] Lemmon, M. A.; Flanagan, J. M.; Hunt, J. F.; Adair, B. D.; Bormann, B.-J.; Dempsey, C. E.; Engelman, D. M. *J Biol Chem* 1992, 267, 7683-7689.
- [11] Lemmon, M. A.; Flanagan, J. M.; Treutlein, H. R.; Zhang, J.; Engelman, D. M. *Biochemistry* 1992, 31, 12719-12725.
- [12] Gottschalk, K. -E.; Kessler, H. *Structure* 2004, 12, 1109-1116.
- [13] Gottschalk, K. -E.; Soskine, M.; Schuldiner, S.; Kessler, H. *Biophys J* 2004, 86, 3335-3348.
- [14] Zhang, C.; Hou, J.; Kim, S. -H. *Proc Natl Acad Sci* 2002, 99, 3581-3585.
- [15] Sale, K.; et al. *Prot Sci* 2004, 13, 2613-2627.
- [16] Delaglio, F.; Kontaxis, G.; Bax, A. *J Amer Chem Soc* 2000, 122, 2142-2143.
- [17] Gardner, K. H.; Rosen, M. K.; Kay, L. E. *Biochemistry* 1997, 36, 1389-1401.
- [18] Gardner, K. H.; Kay, L. E. *Annu Rev Biomol Struct* 1998, 27, 357-406.
- [19] Goto, N. K.; Gardner, K. H.; Mueller, G. A.; Willis, R. C.; Kay, L. E. *J Biomol NMR* 1999, 13, 369-374.
- [20] Popot, J. L.; Engelman, D. M. *Annu Rev Biochem* 2000, 69, 881-922.
- [21] Bormann, B. J.; Engelman, D. M. *Annu Rev Biophys Biomol Struct* 1992, 21, 223-242.
- [22] Lemmon, M. A.; Engelman, D. M. *FEBS Letters* 1994, 346, 17-20.
- [23] MacKenzie, K. R.; Prestegard, J. H.; Engelman, D. M. *Science* 1997, 276, 131-133.
- [24] Fu, D.; Libson, A.; Mierke, L. J.; Weitzman, C.; Nollert, P.; Krucinski, J.; Stroud, R. M. *Science* 2000, 290, 481-486.
- [25] de Groot, B. L.; Engel, A.; Grubmüller, H. *FEBS Lett* 2001, 504, 206-211.
- [26] Sui, H.; Bong-Gyoon, H.; Lee, J. K.; Walian, P.; Jap, B. K. *Nature* 2001, 414, 872-878.
- [27] de Groot, B. L.; Grubmüller, H. *Science* 2001, 294, 2353-2357.
- [28] Tajkhorshid, E. et al *Science* 2002, 296, 525-530.
- [29] Agre, P.; Kozono, D. *FEBS Letters* 555, 72-78.
- [30] Baker, E. N.; Hubbard, R. E. *Prog Biophys Molec Biol* 1984, 44, 97-179.
- [31] Tjandra, N.; Bax, A. *Science* 1997, 278, 1111-1114.
- [32] Prestegard, J. H.; Al-Hashimi, H. M.; Tolman, J. R. *Quarterly Rev Biophys* 2000, 33, 371-424.

- [33] Brünger, A.T. et al Acta Cryst 1998, D54, 905-921.
- [34] Schwieters, C.D.; Kuszewski, J.; Tjandra, N.; Clore, G.M. J. Magn. Reson 2003, 160, 66-74.
- [35] Zweckstetter, M.; Bax, A. J Amer Chem Soc 2000, 122, 3791-3792.
- [36] Choy, W.;Y.; Tollinger, M.; Mueller, G.;A., Kay, L.;E. J. Biomol NMR 2001, 21, 31-40.
- [37] Clore, G. M.; Bewley, C. A. J Magn Reson 2002, 154, 329-335.
- [38] Stein, E. G.; Rice, L. M.; Brunger, A. T. J Magn Res 1997, 124, 154-164.
- [39] Koradi, R.; Billeter, M.; Wüthrich, K. J Mol Graphics 1996, 14, 51-55.
- [40] Ubarretxena-Belandia, I.; Engelman, D. M. Curr Opinion Struct Biol 2001, 11, 370-376.
- [41] von Heijne, G. Quarterly Rev Biophys 1999, 32, 285-307.
- [42] Mesleh, M.; Opella, S. J. J Magn Reson 2003, 163, 288-299.
- [43] Skrynnikov, N. R.; and Kay, L. E. J Biomol NMR 2000, 239-252.
- [44] Gimpelev, M.; Forrest, L. R.; Murray D.; Honig B. Biophys J 2004, 87, 4075-4086.
- [45] Gilson, M. K. Introduction to continuum electrostatics, with molecular applications; Biophysics Textbooks online, 2000.
- [46] Huang, W.; Levitt, D. G., Biophys J 1977, 17, 111-128.
- [47] Hildebrand, P. W.; Preissner, R.; Frömmel, C. FEBS Lett 2004, 559, 145-151.

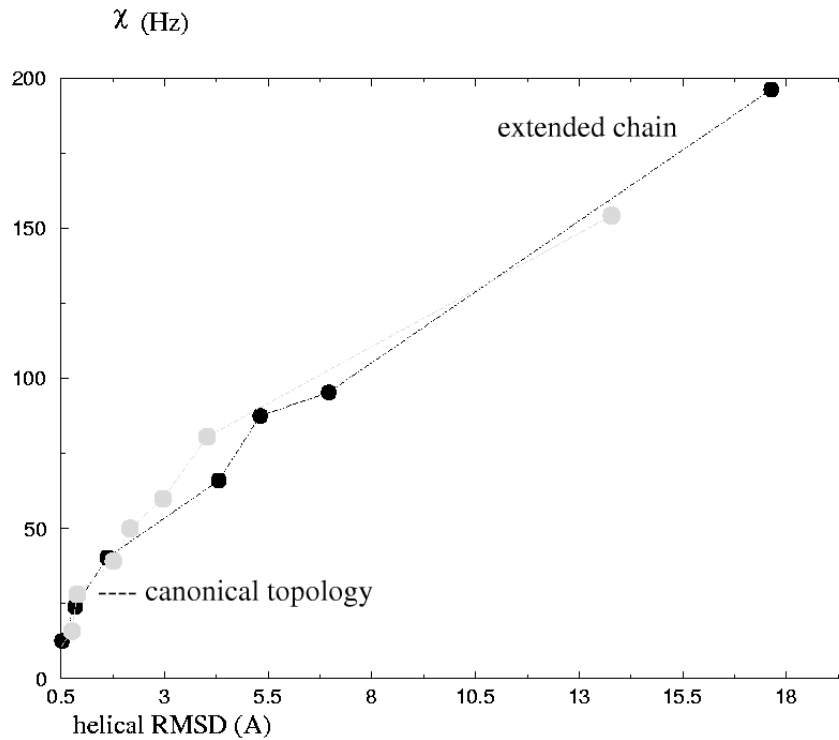


Figure 1: Identification of helical regions from N-H RDC data. The parameter  $\chi$  is plotted for helices with increasing backbone RMSD from the PDB structures. Black circles correspond to the GpA monomer, and grey circles to AQP1 helix 1. RMSD regions corresponding to canonical conformations (generated with imposition of ideal  $\alpha$ -helical dihedral angles and hydrogen bonds), as well as to extended chain conformations, are indicated on the graph.

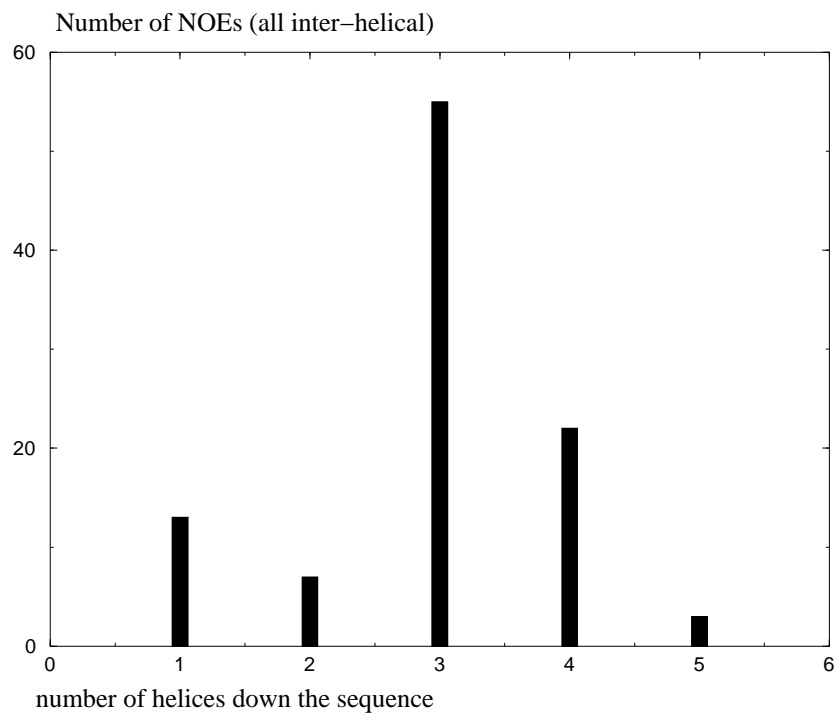


Figure 2: Inter-helical NOE distribution in aquaporin (1J4N), with the selective methyl labeling pattern, as a function of the TM helix consecutivity in the primary sequence.

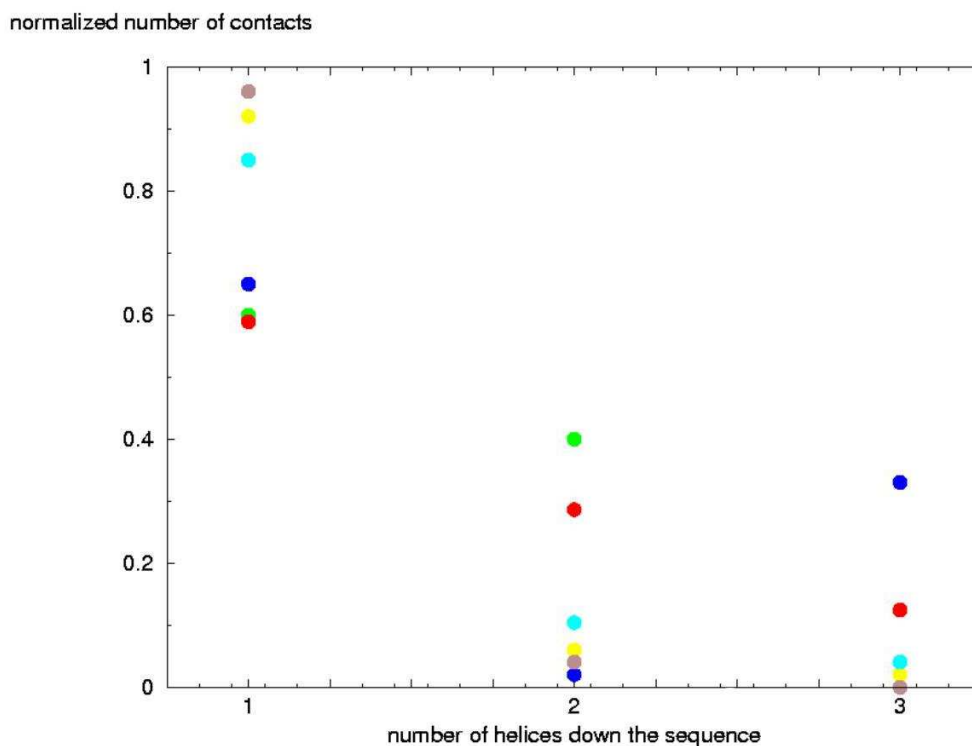


Figure 3: Inter-helical backbone contacts in some transporter/channel proteins: aquaporin (1J4N) in blue, the chloride channel (1KPK) in red, the potassium channel (1BL8) in green, the lactose permease transporter (1PV7) in yellow, the mechanosensitive channel (1MXM) in brown, and the vitamin B12 transporter (1L7V) in cyan. Backbone contacts between TM helices were defined with a cutoff of 6Å (8Å for the mechanosensitive channel, which is very loosely packed), and counted for: adjacent helices ( $n = 1$ ), helices separated by one other TM helix ( $n = 2$ ), and helices separated by two other TM helices in the sequence ( $n = 3$ ). Results are reported as fractions out of the total number of contacts counted for a particular protein. A CNS (Brünger et al, [33]) module was used to identify contacts within a given cutoff.

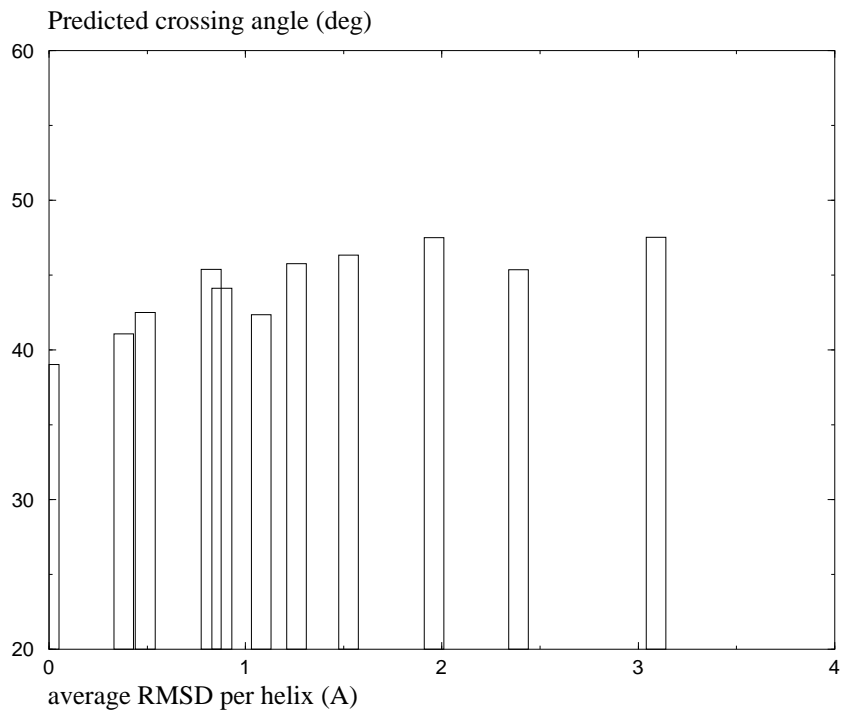


Figure 4: Computation of helix crossing angles in the GpA homodimer, from RDC data simulated for pairs of helices with varying degrees of RMS deviation from the PDB coordinates. For each pair of helices, the crossing angle was calculated using the alignment tensor eigenvectors produced by the Pales ([35]) fit to  $D_{HN}$  RDC data sets computed as described in the text.

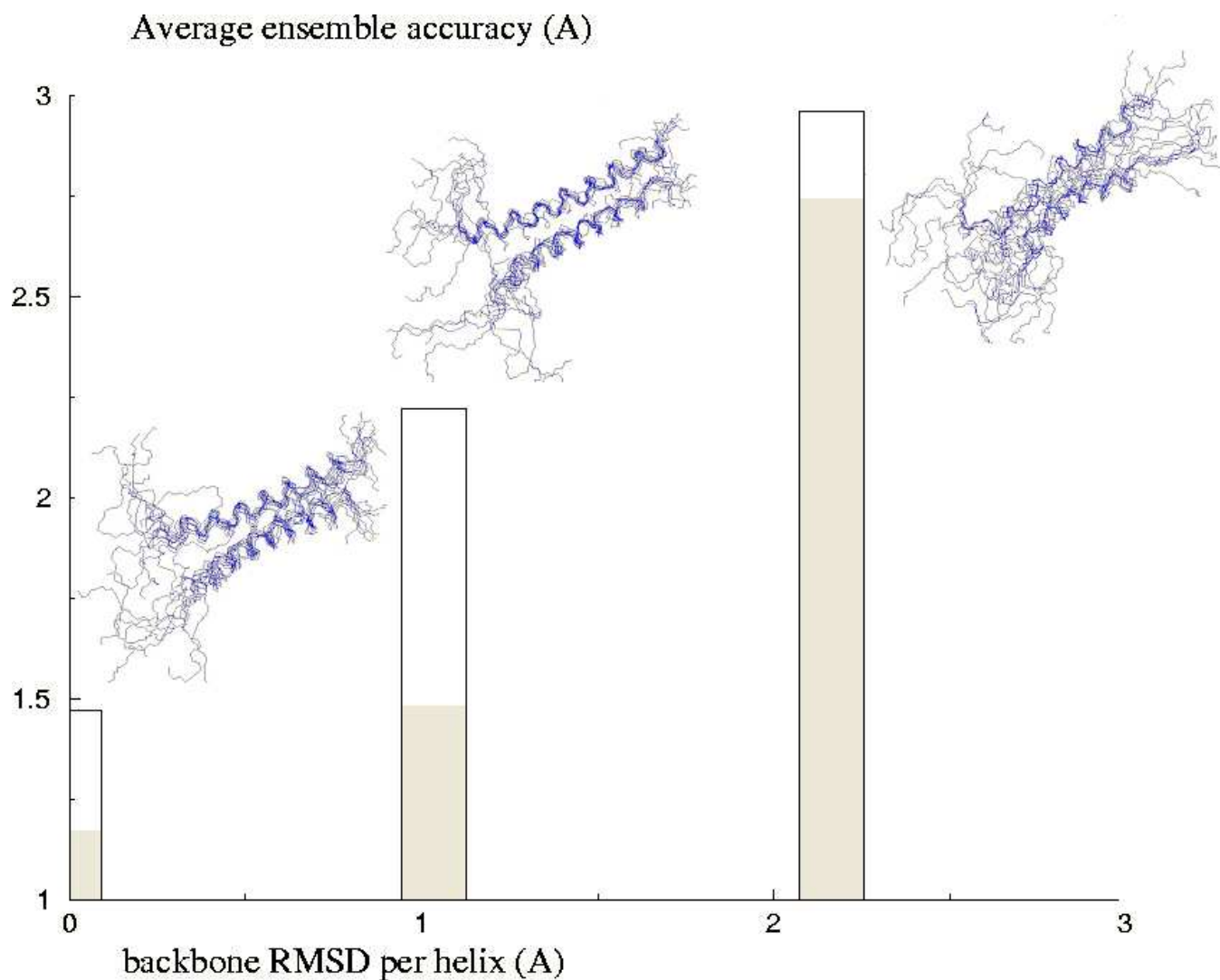


Figure 5: Rigid-body/torsion angle annealing of GpA from pre-folded parallel helices. Dependence of the ensemble accuracy (empty bars) on the average backbone RMS deviation per helix in the starting structure, relative to the reference (PDB) coordinates. Filled bars: average ensemble accuracy of the lowest energy ensemble obtained upon inclusion of a final constant-temperature rigid-body molecular dynamics stage with attractive van der Waals and electrostatic energy terms. Lowest energy rigid-body ensembles are also depicted above the corresponding accuracy/precision plots. The structures correspond to the “SA plus MD” simulations (filled bars).

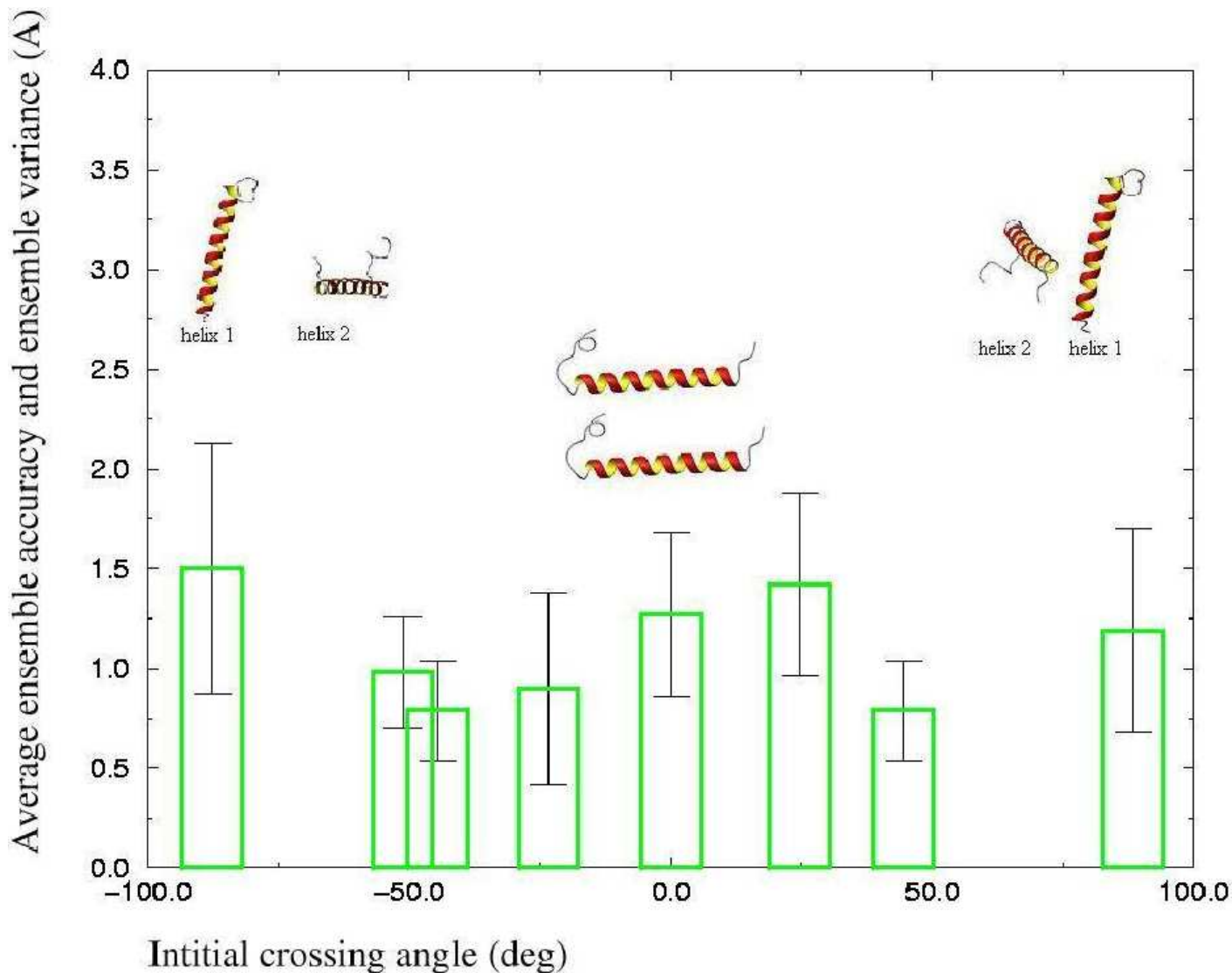


Figure 6: Rigid-body refinement of GpA starting from pre-folded canonical helices, placed initially at various crossing angles. Bars represent average ensemble accuracies on 10 lowest energy structures out of 50 structure ensembles; the variance of the ensemble accuracy is shown in thin lines. Attached on top are the starting structures for the perpendicular ( $\pm 90^\circ$ ) as well as for the parallel helices. Helices are labeled unambiguously, as monomer 1 (left), and 2 (right). The starting helices are obtained from TAD structure calculations with canonical dihedral angles, hydrogen bonds and dipolar couplings, and have an average RMSD of 0.84Å to the PDB helices.

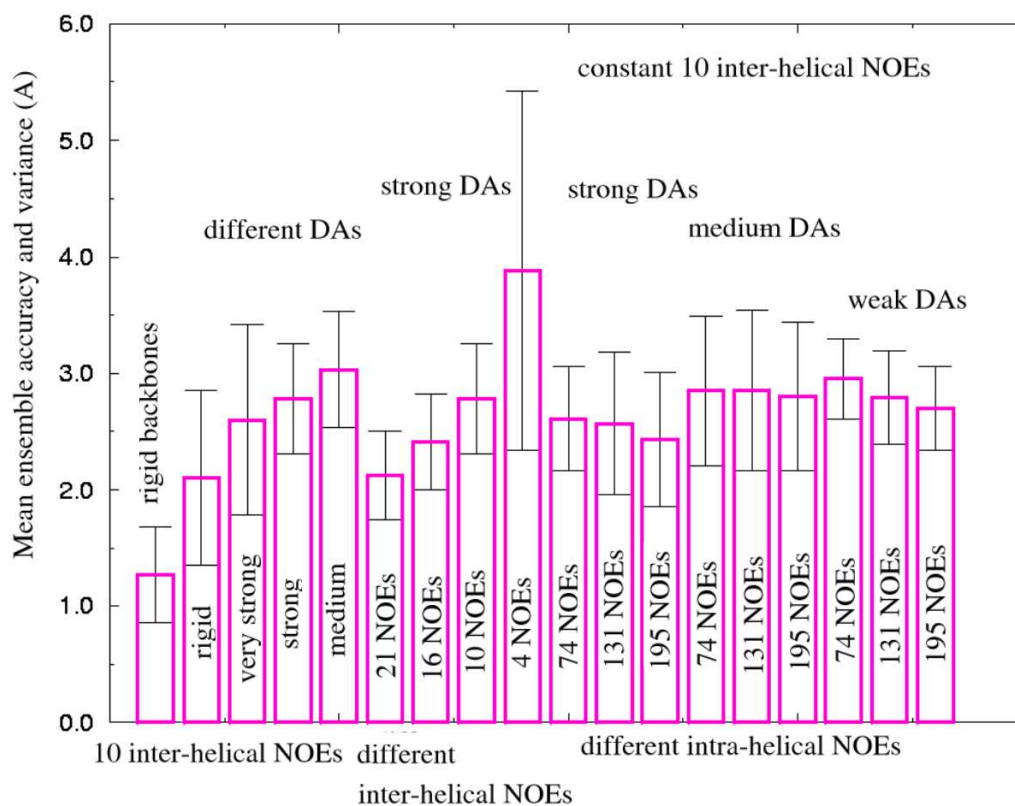


Figure 7: Folding of glycoporphin A

The two methods used are: Rigid-body/torsion angle slow-cooling from a collection of canonical pre-folded TM helices using inter-helical NOE-s, and TAD-simulated annealing from an extended chain conformation with dihedral angle restraints (DA-s), inter-helical NOE-s, and hydrogen bonds (HB-s). With both methods, mean ensemble accuracy and ensemble variance are reported on 10 lowest energy structures out of 100. DA imposition is labeled as follows: rigid - ( $0^\circ$ ,  $0^\circ$ ) bounds around canonical  $\alpha$ -helical dihedrals, very strong - ( $\pm 2.5^\circ$ ,  $\pm 5^\circ$ ) bounds, strong - ( $\pm 10^\circ$ ,  $\pm 20^\circ$ ) bounds, medium - ( $\pm 20^\circ$ ,  $\pm 30^\circ$ ) bounds, and weak - ( $\pm 40^\circ$ ,  $\pm 60^\circ$ ) bounds.

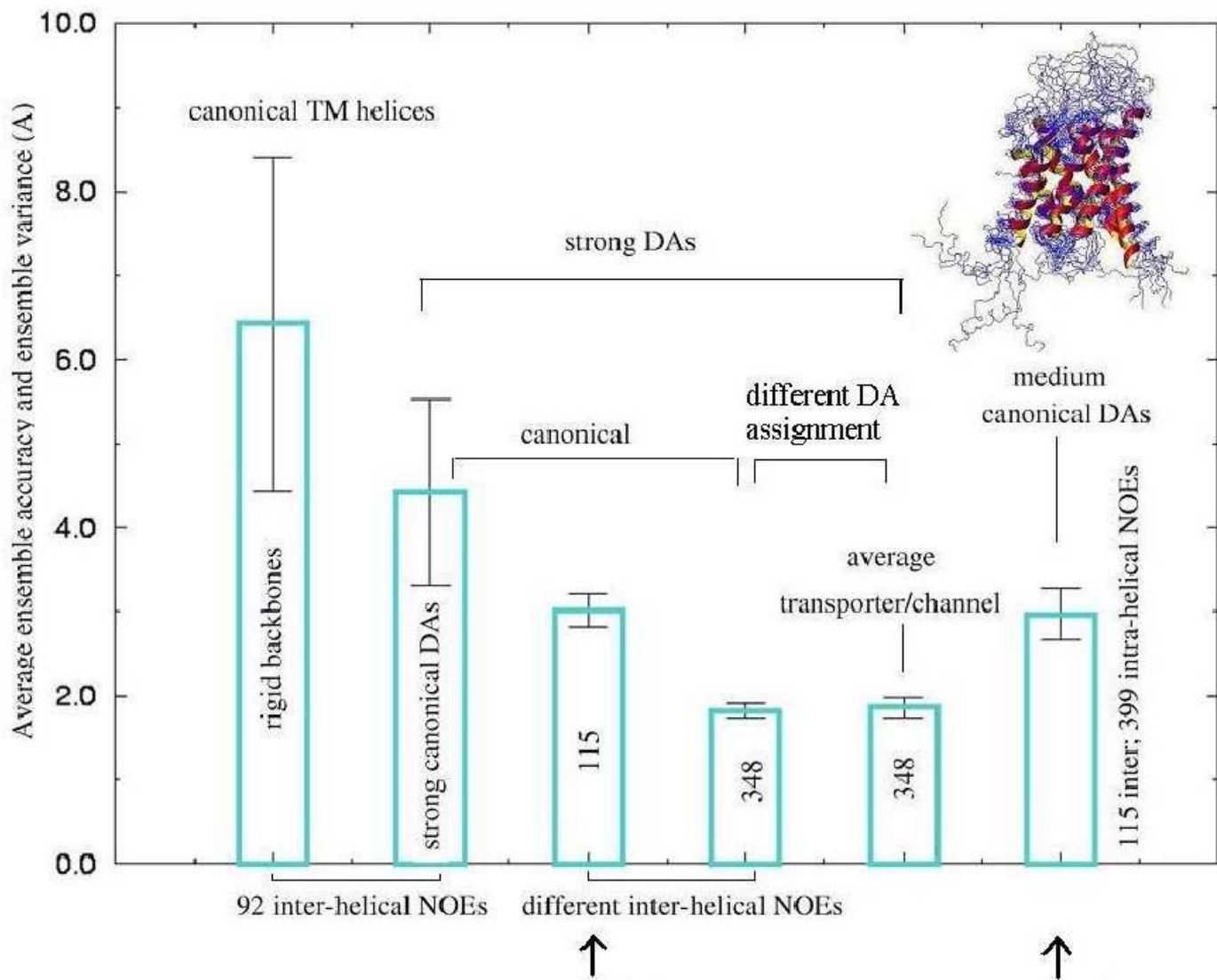


Figure 8: Folding of the water channel

The two methods used are: Rigid-body/torsion angle slow-cooling from a collection of 6 canonical pre-folded TM helices, with 92 inter-helical NOE-s, and TAD-simulated annealing from an extended chain conformation with dihedral angle restraints (DA-s), inter-helical NOE-s, and hydrogen bonds (HB-s). DA restraints are labeled as in Fig.7 (strong and medium). The target values and bounds for the transporter/channel-specific DA-s are given in the text. The depicted ensemble corresponds to test 3 (strong canonical DA-s, 115 inter-helical NOE-s). Accuracies are computed on backbone atoms from the 6 TM helices for the first two tests, and for backbone atoms from 6 + 2 helices for the subsequent tests (including the 2 non-spanning helices). Arrows identify structures calculated with the same inter-helical NOE-s and with or without intra-helical NOE-s.